

Oxygen Moment Formation and Canting in Li_2CuO_2

E.M.L Chung,¹ G.J. McIntyre,² D. McK. Paul,¹ G. Balakrishnan,¹ and M.R. Lees¹

¹*Department of Physics, University of Warwick, Coventry, CV4 7AL, UK*

²*Institut Laue Langevin, BP 156, 38042, Grenoble Cedex 9, France*

(Dated: November 13, 2018)

The possibilities of oxygen moment formation and canting in the quasi-1D cuprate Li_2CuO_2 are investigated using single crystal neutron diffraction at 2 K. The observed magnetic intensities could not be explained without the inclusion of a large ordered oxygen moment of $0.11(1) \mu_B$. Least-squares refinement of the magnetic structure of Li_2CuO_2 in combination with a spin-density Patterson analysis shows that the magnetization densities of the Cu and O atoms are highly aspherical, forming quasi-1D ribbons of localised Cu and O moments. Magnetic structure refinements and low-field magnetization measurements both suggest that the magnetic structure of Li_2CuO_2 at 2 K may be canted. A possible model for the canted configuration is proposed.

PACS numbers: 61.12.-q, 75.25.+z, 75.30.-m, 75.40.Cx

I. INTRODUCTION

Quasi-one-dimensional cuprates such as Li_2CuO_2 exhibit a wide range of interesting electronic and magnetic properties. As Li_2CuO_2 possesses 1D chains of $S=\frac{1}{2}$ copper atoms it serves as a useful model system for studies of low dimensional behavior and quantum fluctuations in the spin $\frac{1}{2}$ quantum chain. Also embedded within the chemical structure of Li_2CuO_2 are sets of parallel Cu-O₂ ribbons (figure 1), similar to those found in the spin-Peierls compound CuGeO_3 and chain-ladder system $\text{La}_{14-x}\text{Ca}_x\text{Cu}_{24}\text{O}_{41}$. Li_2CuO_2 therefore also frequently serves as a model system for investigation of the electronic structure and correlations of the Cu-O₂ ribbon^{1,2,3,4,5}.

The Cu-O networks of Li_2CuO_2 , CuGeO_3 , high- T_C materials and many other cuprates can be thought of as being constructed from the same basic building block; a CuO_4 plaquette. In high- T_C compounds, the plaquettes are corner sharing forming 2D planes, whilst in Li_2CuO_2 and CuGeO_3 they are edge-sharing, forming Cu-O ribbons. The magnetic properties of cuprates are known to be crucially dependent upon the Cu-O-Cu bond angle linking nearest neighboring Cu atoms. When this angle approaches 90° the strength of the superexchange interaction diminishes and a change in magnetic ordering from antiferromagnetic (AFM) to ferromagnetic (FM) occurs^{6,7,8}. In the context of other cuprates Li_2CuO_2 is unusually placed since it possesses a Cu-O-Cu exchange pathway of 94° . This angle is close to the crossover region between AFM and FM ordering and frustration effects resulting from competing interactions are anticipated.

Local spin-density approximation (LSDA)^{1,4} and quantum chemical⁵ calculations have recently suggested that the oxygen ions may play a more novel and fundamental role in the magnetism of Li_2CuO_2 than previously thought. The LSDA calculations suggest an ordered magnetic moment of $0.92 \mu_B$ per formula unit, 40% of which is predicted to be associated with the ‘non-

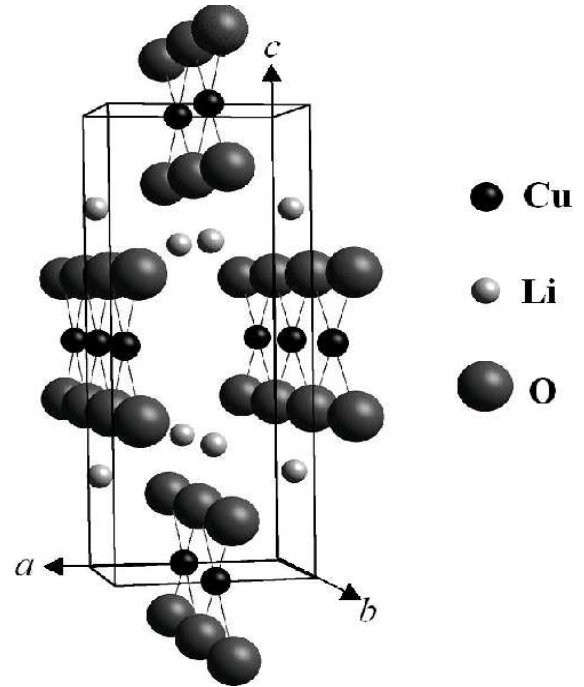


FIG. 1: Chemical structure of Li_2CuO_2 showing the CuO_2 ribbons created along b by an edge-sharing arrangement of CuO_4 plaquettes.

magnetic’ oxygen sites¹. Although covalency effects (e.g. in K_2IrCl_6)⁹ are not unknown, a moment as large as $0.2 \mu_B$ associated with each of the oxygen sites would be unprecedented. A more conservative estimate of the oxygen moment is provided by quantum chemical techniques, however, these values vary dramatically (from 0.03 to $0.17 \mu_B$) depending upon which approximations have been employed to treat the electronic correlations.

Previous studies on polycrystalline Li_2CuO_2 include the determination of the crystal structure via X-rays¹⁰, and the observation of an antiferromagnetic ordering

temperature of $T_N \simeq 9$ K^{11,12,13}. Early neutron diffraction investigations performed on powder samples at 1.5 K suggested a collinear arrangement of moments coupled ferromagnetically within the a - b plane, and antiferromagnetically in the c -direction^{14,15}. A magnetic moment of $0.96(4) \mu_B$ was estimated and attributed solely to the magnetic Cu^{2+} ions¹⁵. Electron paramagnetic resonance and antiferromagnetic resonance experiments showed that the easy axis for the spins lies along the a -direction¹¹.

More recently, single-crystal muon spectroscopy and powder susceptibility measurements have indicated that in weak fields the magnetic structure of Li_2CuO_2 below 2.6 K may be canted away from the a -axis^{16,17}. The temperature dependence of the internal fields probed by μSR also suggests that there may be magnetic moments on both the Cu and the O ions¹⁶.

An excellent test of the reported magnetic structure, and of the validity of Li_2CuO_2 LSDA predictions, can be found through measurement of the magnetic moment associated with each atom of Li_2CuO_2 using single-crystal neutron diffraction. By this method it is possible to survey efficiently several hundred magnetic and nuclear reflections over a large volume of reciprocal space, enabling the magnetic structure of Li_2CuO_2 to be determined with good statistical accuracy.

In this paper, the growth and characterization of Li_2CuO_2 single crystals, and experimental details of our neutron-scattering measurements are first described. In section III the Li_2CuO_2 magnetic form factor and spin-density Patterson functions are introduced. Patterson analysis of our observed Li_2CuO_2 magnetic diffraction pattern reveals the existence of a large moment associated with the oxygen sites. Section IV contains the results of least-squares refinement of the magnetic structure of Li_2CuO_2 with respect to various magnetic models. Despite complications introduced by a possible slight canting of the Cu and O moments, all models consistently estimate that the magnitude of the oxygen moment lies between $0.10 \mu_B$ and $0.12 \mu_B$. Lastly, our magnetic model of Li_2CuO_2 is refined further to include the possibility of canting. Section V contains an additional investigation of the canted phase, performed using heat capacity and single-crystal magnetization measurements.

II. EXPERIMENTAL DETAILS

Single crystals of Li_2CuO_2 were grown from phase-pure polycrystalline Li_2CuO_2 ¹⁸ using a four-ellipsoid floating-zone furnace at a rate of 3-6 mm/h in 1.3 atm of flowing oxygen. The resulting crystalline boules were faceted and possessed a pronounced tendency to cleave along parallel (101) planes.

Room-temperature powder X-ray diffraction patterns obtained for finely-crushed portions of our Li_2CuO_2 single-crystals showed that the samples were of high purity. All peaks were indexed in the orthorhombic

space group $Immm$ and our single crystals exhibited all of the expected bulk magnetic properties (susceptibility and heat capacity) associated with the onset of three-dimensional antiferromagnetic order at $T_N = 9 \pm 0.1$ K (figure 7, discussed in section V).

Neutron diffraction measurements were performed at the high-flux reactor at the Institut Laue Langevin (ILL), Grenoble, using the D10 diffractometer in its four-circle configuration with an offset Eulerian cradle, He-flow cryostat and position-sensitive 80×80 mm² area detector. The 40 mg single crystal platelet of Li_2CuO_2 had (101) flat faces of area 3×4 mm² spaced 0.3 mm apart. The positions and intensities of all accessible nuclear and magnetic reflections with $k \geq 0$ were scanned at 2 K using a constant neutron wavelength of $1.257(5)$ Å to give up to four symmetry equivalents for each unique reflection.

Background subtraction and peak integration were performed using the “*minimum in $\sigma(I)/I$ method*”¹⁹ where statistically optimum results are obtained in the integration of weaker magnetic reflections by using three-dimensional profiles estimated from stronger neighboring reflections. The data were corrected for absorption²⁰ using an calculated absorption coefficient of 0.2114 mm⁻¹. The transmission factors ranged from 41.7% to 87.7% depending on orientation. Examination of the intensities of the stronger nuclear reflections suggested that measurements of the nuclear peaks had suffered significantly from extinction. The extinction could be accounted for reasonably well in the structure refinements using a Becker and Coppens type I Lorentzian model²¹, with a crystal mosaicity of $0.03(2)^\circ$.

III. THE MAGNETIC FORM FACTOR

Below T_N , magnetic peaks develop at $h+k+l=2n+1$ (indexed on the basis of the nuclear unit-cell), due to the antiferromagnetic ordering of Cu moments positioned at $(0,0,0)$ and $(\frac{1}{2}, \frac{1}{2}, \frac{1}{2})$. Assuming that all of the magnetic scattering arises from the Cu atoms the magnetic intensity can be described by,

$$I_M(\mathbf{Q}) \propto T^2 |G(\mathbf{Q}) f_m(\mathbf{Q}) (1 - e^{-2\pi i(\frac{h}{2} + \frac{k}{2} + \frac{l}{2})})|^2 \quad (1)$$

‘ T ’ is a temperature factor, whose variation with Q at 2 K can be ignored, and $f_m(\mathbf{Q})$ is the atomic magnetic form factor of the Cu site. Assuming that the moments are oriented along the a -axis the geometrical orientation factor, $G(\mathbf{Q})$, for this orthorhombic cell is given by,

$$G(\mathbf{Q}) = \frac{\sqrt{(\frac{k}{b})^2 + (\frac{l}{c})^2}}{\sqrt{(\frac{h}{a})^2 + (\frac{k}{b})^2 + (\frac{l}{c})^2}} \quad (2)$$

thus, apart from some constant scale factors the magnetic form factor can be extracted using,

$$f_m(\mathbf{Q}) \propto \sqrt{I_M(\mathbf{Q})/|G(\mathbf{Q})|^2} \quad (3)$$

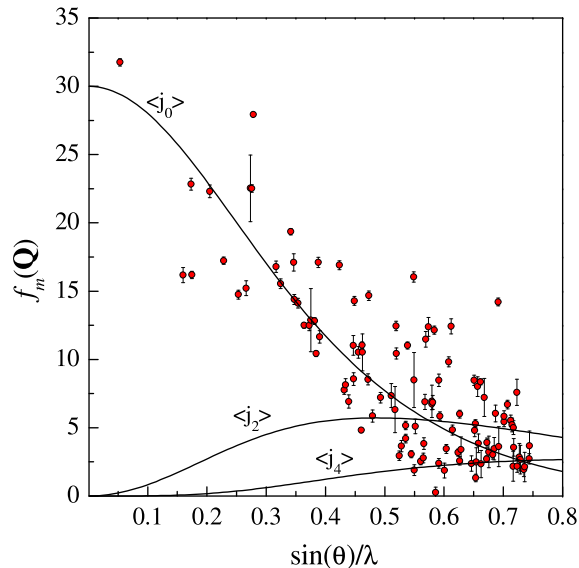


FIG. 2: The magnetic form-factor of Li_2CuO_2 (markers), calculated from the observed data by assuming a model of a -axis Cu moments. The lines depict the $\langle j_0 \rangle$, $\langle j_2 \rangle$ and $\langle j_4 \rangle$ radial integrals for the free Cu^{2+} ion²² (scaled).

The magnetic form factor of Li_2CuO_2 , calculated from the measured intensities by assuming that magnetic scattering arises exclusively from a -axis Cu moments is plotted in figure 2. It can be seen that our measurements deviate radically from the $\langle j_0 \rangle$ radial integral for the free Cu^{2+} ion²². This is to be expected because of the effects of crystalline anisotropy on the magnetization density close to the Cu sites. A further departure from spherical symmetry may also arise due to the presence of a magnetic moment elsewhere in the unit cell, such as on the oxygen sites.

It should be noted that if a large oxygen moment exists, or the spins in Li_2CuO_2 are significantly canted, the expression for $G(\mathbf{Q})$ (provided in equation 2) will no longer represent a good approximation for the geometrical orientation factor. In this situation, the values estimated for $f_m(\mathbf{Q})$ (using equation 3) could differ considerably from those plotted.

A. The Spin-density Patterson Function

In principle, the three-dimensional real-space magnetization density of the crystal may be obtained directly through Fourier transformation (F.T.) of the complete magnetic structure factor, $\mathbf{F}_M(\mathbf{Q})$. The full magnetic structure factor is a vector quantity that carries information about the magnitude *and* the direction of the spin-density at every point in the unit cell.

$$\rho_m(\mathbf{r}) = \text{F.T.}[\mathbf{F}_M(\mathbf{Q})] \quad (4)$$

Unfortunately, analysis of our neutron diffraction data by this method is hindered by the lack of phase information. Since unambiguous knowledge of the phase of each of the reflections was unavailable a magnetic Patterson approach was adopted^{23,24,25}. Unlike maximum entropy methods, Patterson analysis requires no phase information, or prior knowledge of the positions or the directions of the moments. The spin-density Patterson approach treats the magnetic structure as being completely unknown.

The Patterson function was first introduced in 1934, and has become an invaluable tool for the determination of unknown crystal structures principally via X-rays. The non-magnetic Patterson function represents the autocorrelation function of the electron density in the unit cell, and is defined as the Fourier transform of the squared nuclear structure factor,

$$P_N(\mathbf{u}) = \text{F.T.}[|F_N(\mathbf{Q})|^2] \quad (5)$$

$$P_N(\mathbf{u}) = \rho_n(\mathbf{r}) \otimes \rho_n(-\mathbf{r}) \quad (6)$$

The nuclear Patterson function, $P_N(\mathbf{u})$, provides a map of the vectors between *pairs* of atoms in the unit cell. (i.e. in a unit cell containing n atoms, each atom will form a pair with all atoms, including itself, producing n^2 Patterson peaks).

The relationship between the magnetic Patterson function and the unpaired spin-density is not as trivial as the situation described for the nuclear Patterson function. The dipolar nature of the electron-neutron interaction means that the intensity of magnetic scattering is governed by the relative orientation of the spins and the scattering vector (\mathbf{Q}). In terms of $\mathbf{F}_M(\mathbf{Q})$ neutrons are scattered by the sample with an intensity given by²⁶,

$$I_M(\mathbf{Q}) \propto |\mathbf{F}_M(\mathbf{Q})|^2 - |\hat{\mathbf{Q}} \cdot \mathbf{F}_M(\mathbf{Q})|^2 \quad (7)$$

Where $\hat{\mathbf{Q}}$ represents a unit vector in the direction of \mathbf{Q} . Calculation of the spin-density Patterson map by Fourier transformation of the measured magnetic intensities (equation 8) generates a plot of the pair-correlation function between magnetic scatterers, equation 9,

$$P_M(\mathbf{u}) \propto \text{F.T.}[|\mathbf{F}_M(\mathbf{Q})|^2] - \text{F.T.}[|\hat{\mathbf{Q}} \cdot \mathbf{F}_M(\mathbf{Q})|^2] \quad (8)$$

$$P_M(\mathbf{u}) = \sum_{i=1}^3 \sum_{j=1}^3 (\rho_i(\mathbf{r}) \otimes \rho_j(-\mathbf{r})) - \sum_{i=1}^3 \sum_{j=1}^3 \text{F.T.}[\hat{Q}_i \hat{Q}_j] \otimes (\rho_i(\mathbf{r}) \otimes \rho_j(-\mathbf{r})) \quad (9)$$

The three spatial components of spin density of the i 'th and j 'th atoms have been written as summations over ρ_i and ρ_j . $\hat{Q}_i \hat{Q}_j$ describes the product of the magnitudes of the i 'th and j 'th components of the unit vector $\hat{\mathbf{Q}}$. The symbol \otimes denotes a convolution.

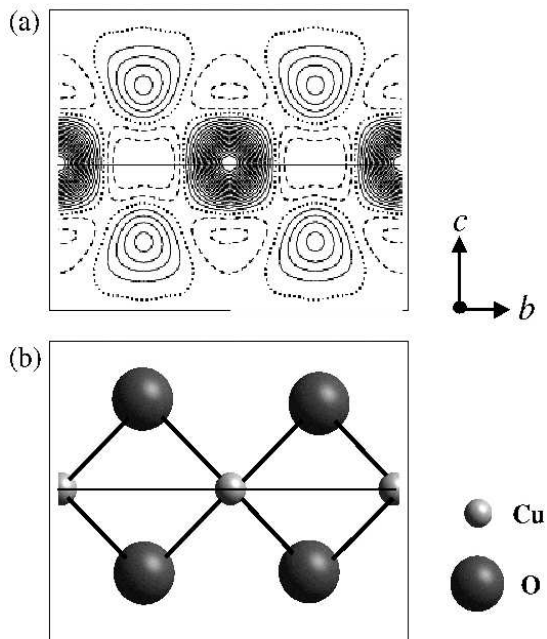


FIG. 3: (a) The magnetic Patterson section generated from the observed data ($|F_M(hkl)|^2$), viewed as a $(\frac{1}{2} b c)$ slice through the Li_2CuO_2 unit cell. Note that significant magnetic intensity is associated with inter-atomic vectors between copper and oxygen sites. This confirms the presence of unpaired spins on the oxygen sites, see equation 10. Filled, dotted and dashed lines represent positive, zero and negative contours respectively. Contours extend from -5 to 50 in 2.5 steps. (b) The corresponding positions of the atoms in the Li_2CuO_2 unit cell.

The second term in equation 9 probes the directions of the moments, causing the Patterson peaks to become elongated along the direction parallel to the vector bisector between spins. Full details of this theory, and references relating the uses of the Patterson function in magnetism can be found in the references^{23,24,25}.

B. Li_2CuO_2 Spin-density Patterson Analysis

For the purposes of Patterson analysis, the Li_2CuO_2 magnetic data set of 409 observations was reduced to a complete set of 111 averaged unique reflections. Including the possibility of magnetic oxygen sites there are $n=6$ magnetic atoms per chemical unit cell producing $n^2 = 36$ Patterson peaks. The heights of the 36 peaks may be represented by a symmetric matrix \mathbf{P} . Each matrix element corresponds to the scalar product of pairs of spins at sites i and j .

$$\mathbf{P} = \begin{pmatrix} \mathbf{S}_{Cu1} \cdot \mathbf{S}_{Cu1} & \mathbf{S}_{Cu1} \cdot \mathbf{S}_{Cu2} & \dots & \mathbf{S}_{Cu1} \cdot \mathbf{S}_{O4} \\ \mathbf{S}_{Cu2} \cdot \mathbf{S}_{Cu1} & \mathbf{S}_{Cu2} \cdot \mathbf{S}_{Cu2} & & \vdots \\ \vdots & & \ddots & \vdots \\ \mathbf{S}_{O4} \cdot \mathbf{S}_{Cu1} & \dots & \dots & \mathbf{S}_{O4} \cdot \mathbf{S}_{O4} \end{pmatrix} \quad (10)$$

In interpreting the spin-density Patterson function it should be remembered that the positions of the peaks correspond to the interatomic vectors *between* scatterers rather than the positions of the scatterers themselves. A large origin peak containing overlapping contributions from n diagonal matrix elements, $(\mathbf{S}_n \cdot \mathbf{S}_n)$, occurs due to the convolution of each magnetic site with itself. With a knowledge of the chemical structure, it is possible to relate the stronger peaks, dominated by $\mathbf{S}_{Cu} \cdot \mathbf{S}_{Cu}$ terms, to interatomic vectors between the centrosymmetric positions of the Cu sites. Since there are only two Cu atoms per unit cell (related by body centering), any peaks in addition to those at $(0,0,0)$ and $(\frac{1}{2}, \frac{1}{2}, \frac{1}{2})$ must represent additional interatomic vectors between Cu sites and other magnetic scatterers.

In the observed Patterson map (figures 3 and 4) additional peaks are observed at positions that do not correspond to inter-atomic Cu vectors. Comparison with the positions of the atoms in the unit cell shows that a considerable number of the magnetic scatterers are closely associated with the crystallographic positions of the oxygen atoms. (These peaks are dominated by $\mathbf{S}_{Cu} \cdot \mathbf{S}_O$ terms). Asymmetry in the magnetic Patterson peaks in the immediate vicinity of the O sites (as viewed along the a -axis) is in good agreement with the exchange potential $(V_\uparrow - V_\downarrow)$ predicted for the ferromagnetic Cu-O chain by LSDA calculations¹.

A three-dimensional Patterson plot of the observed data is provided in figure 4. A reversal in sign between CuO_4 units positioned at $(0,0,0)$ and $(\frac{1}{2}, \frac{1}{2}, \frac{1}{2})$ is observed. Elongation of the peaks along the a -direction is consistent with the direction of the bisector of the spins being parallel to the a -axis, which does not exclude the possibility of canting.

IV. LEAST-SQUARES REFINEMENT

Although Patterson analysis has proved useful for locating the distribution of spin-density in the Li_2CuO_2 unit cell, an estimate has not so far been obtained for the magnitudes and directions of the spins. A quantitative estimation of the magnitude of the moments in Li_2CuO_2 can be gained through least-squares refinement of the magnetic data set with respect to an appropriate magnetic model (or models).

Before refining the magnetic structure of Li_2CuO_2 the nuclear structure was verified using the CCSL program SFLSQ²⁷. The nuclear data set consisted of 445 reflections ($h+k+l=2n$) measured at 2 K. The atomic positions and thermal parameters resulting from refinement

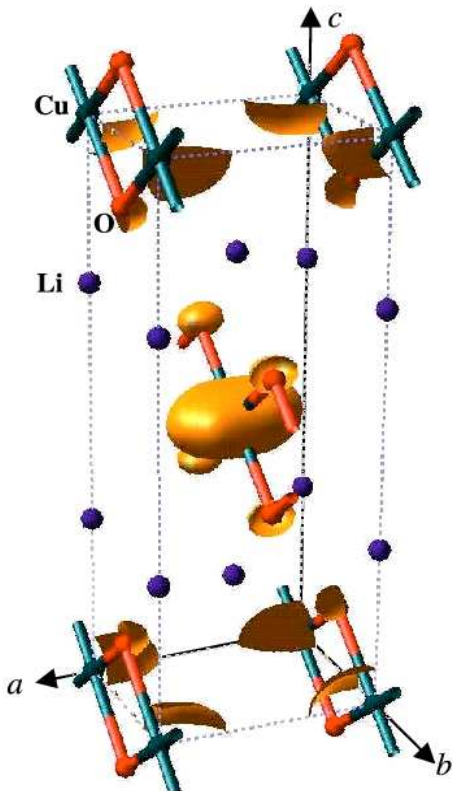


FIG. 4: Three-dimensional Patterson map superimposed upon the Li_2CuO_2 unit cell. Contours at $(0,0,0)$ and $(\frac{1}{2}, \frac{1}{2}, \frac{1}{2})$ are fixed at values of +45 and -45 respectively, (illustrating the reversal in sign between spins at $(0,0,0)$ and $(\frac{1}{2}, \frac{1}{2}, \frac{1}{2})$).

of the data are provided in Table I. Unit cell parameters at 2 K were refined to be $a=3.661(4)$, $b=2.866(7)$, and $c=9.397(8)$ Å. The high value of $\chi^2=17.9$ is likely to be due to extinction effects that have not been perfectly corrected by the Becker-Coppens procedure.

TABLE I: Li_2CuO_2 atomic positions and thermal parameters measured at 2 K, obtained through the refinement of 9 basic variables, $\chi^2=17.9$, $R(F)=2.15$. ($R(F) = \sum |F_0 - F_C| / \sum |F_0|$ and $\chi^2 = \frac{1}{n-p} \sum w(F_O^2 - F_C^2)$, where n is the number of points, p the number of parameters and w the weighting.) Thermal parameters, (assumed to be isotropic for Li and Cu, and anisotropic for O,) correspond to the expression $\exp[-(h^2\beta_{11} + k^2\beta_{22} + l^2\beta_{33})]$.

Atom	X	Y	Z	Thermal parameters
Li	0	0	0.7132(2)	$\beta_{11} = \beta_{22} = \beta_{33} = 0.326(20)$
Cu	0	0	0	$\beta_{11} = \beta_{22} = \beta_{33} = 0.095(10)$
				$\beta_{11} = 0.279(14)$
O	0.5	0	0.6421(5)	$\beta_{22} = 0.161(16)$
				$\beta_{33} = 0.229(15)$

Refinement of the magnetic structure of Li_2CuO_2 was performed using the CCSL programs MAGLSQ and MM-

PLSQ. The atomic co-ordinates, thermal displacement parameters and overall scale factor were fixed to the values found from refinement against the nuclear reflections (table I). Calculated magnetic form factors were assumed for the copper²² and oxygen^{22,28} sites. As preliminary refinements showed that extinction corrections for the magnetic peaks were negligible, the magnetic reflections could be grouped and averaged.

For completeness, refinement of the magnetic structure of Li_2CuO_2 was first carried out by assuming a model based upon previous reports - an antiferromagnetic arrangement of a -axis Cu moments^{11,14,15}. Refinements based on this model (with spherical form-factors) estimated an a -axis Cu moment of $0.938 \pm 0.024 \mu_B$. This value is close to the $0.96 \mu_B$ estimated from powder neutron diffraction¹⁵. However, considering that there are no extinction effects associated with the magnetic reflections, the model provides a poor fit to the data ($\chi^2 = 45$), see figure 5(a). A number of model structures containing canted copper moments were also investigated but none were found that enhanced the refinement. Tilting of the Cu moments away from the a -axis in itself was not sufficient to explain the observed magnetic intensities.

A more satisfactory fit to the data ($\chi^2=31$) could be achieved through the inclusion of an ordered oxygen moment, see figure 5(b). Comparison of the Patterson map generated using this model with the observed Patterson map in figure 3(a) shows that the magnetization densities of the Cu and O sites are asymmetric in the b - c plane. This strongly indicates the importance of aspherical multipolar contributions.

Asymmetry in the magnetization densities of the Cu and O sites was modeled using linear combinations of spherical harmonics. The angular dependence of the magnetization density of the centro-symmetric Cu sites was modeled using an approximation of the form of Equation 11, where the radial integrals $\langle j_0 \rangle$, $\langle j_2 \rangle$ and $\langle j_4 \rangle$ (as shown in figure 2) are now modified to possess an angular dependence expressed in terms of Bessel functions $Y[l, m]$. The non-centrosymmetric O angular dependence was modeled using an approximation in the form of equation 12. The coefficients $a_{l,m}$ are fitted parameters determined during the refinement.

$$\rho_{Cu} = a_{0,0} \langle j_0 \rangle + a_{2,0} \langle j_2 \rangle Y[2, 0] + \langle j_4 \rangle (a_{4,0} Y[4, 0] + a_{4,2} Y[4, 2^+]) \quad (11)$$

$$\rho_O = a_{0,0} \langle j_0 \rangle + a_{1,0} \langle j_1 \rangle Y[1, 0] + \langle j_2 \rangle a_{2,2} Y[2, 2^+] \quad (12)$$

Sequential introduction of aspherical form factors into our model, refined with MMPLSQ, was found to improve the fit remarkably. The Patterson section along the Cu-O chain, obtained using data calculated by assuming a model containing aspherical Cu and O form-factors, is depicted in figure 5(c). Spherical harmonics that did not

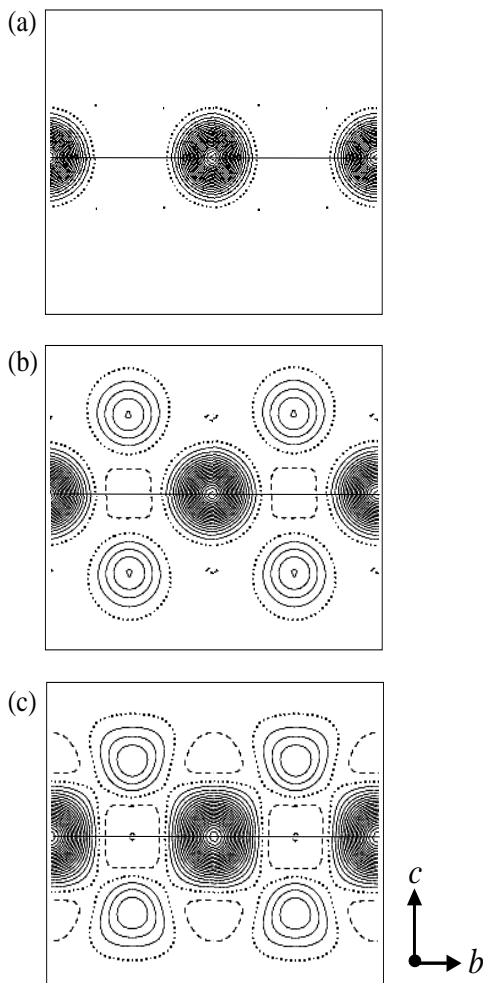


FIG. 5: Magnetic Patterson sections taken through the Cu-O ribbon, generated from least-squares refined model data. Figure 5(a) spherical a -axis Cu moments. Fig. 5(b) spherical a -axis Cu and O moments. Fig. 5 (c) non-spherical a -axis Cu and O moments. For comparison, the observed Patterson map is provided in fig.3.

contribute significantly were omitted from the final refinement.

A summary of the results of analysis of the magnetic dataset using a variety of starting models is presented in table II. Spherical harmonics introduced to model the magnetization densities of the Cu and O sites are indicated by the values of $Y[l,m]$. (For example, $Y[0,0]$ indicates that the magnetization density was assumed to be perfectly spherical.) The magnitude of the O moment, refined to be approximately $0.11 \mu_B$ in size, remained stable throughout the refinements. These O moments are coupled to Cu moments between $0.91 \mu_B$ and $0.96 \mu_B$ in size.

TABLE II: Li_2CuO_2 magnetic structure refinements performed on a unique set of 111 reflections. Spherical harmonics introduced to model the magnetization densities of the Cu and O sites are indicated by the values of $Y[l,m]$, (where l and m denote electronic quantum numbers). θ is the angle away from c^* ; ϕ is the angle to a^* in the a - b plane.

MODEL	Cu (μ_B)	O (μ_B)	χ^2
a -axis Cu	0.938	–	44.9
Cu: $Y[0,0]$	± 0.024		
a -axis Cu & O,	0.911	0.105	30.7
Cu, O: $Y[0,0]$	± 0.021	± 0.012	
a -axis Cu & O			
Cu: $Y[0,0]$, $Y[2,*]$ & $Y[4,*]$	0.960	0.100	15.7
O: $Y[0,0]$	± 0.017	± 0.008	
a -axis Cu & O,			
Cu: $Y[0,0]$, $Y[2,*]$ & $Y[4,*]$	0.963	0.105	11.1
O: $Y[0,0]$, $Y[1,0]$ & $Y[2,2^+]$	± 0.014	± 0.007	
Canted(θ, ϕ):			
Cu($76^\circ, 0^\circ$), O($116^\circ, 0^\circ$),			
Cu: $Y[0,0]$, $Y[2,*]$ & $Y[4,*]$	0.914	0.116	8.75
O: $Y[0,0]$, $Y[1,0]$ & $Y[2,2^+]$	± 0.006	± 0.004	

A. Canting

Although asphericity can be seen to play an important role in describing the magnetism of Li_2CuO_2 , the high value of $\chi^2=11.1$ indicates that further information can be extracted from the data. Difficulties encountered during refinement of the magnetic structure of Li_2CuO_2 may be explained by mounting evidence suggesting that below $T = 2.6 \pm 0.2$ K the moments are slightly canted^{16,17}. Other than the transition temperature, little is known about the nature of the canted phase, except that the canting angle is likely to be in excess of 0.7° ¹⁶.

In the present study we consider the possibility of an *antiferromagnetic* canted arrangement of moments. (In an antiferromagnetically canted arrangement the moments are tilted so that the net magnetization in all directions remains zero, and no magnetic intensity is contributed to the positions of the nuclear peaks.) This restriction seems reasonable considering the absence of a second transition in the temperature dependence of the (012) and (001) peaks, figure 7(c). To the best of our knowledge no evidence exists in support of a ferromagnetically canted arrangement of moments in zero-field. Canting of the moments towards the c -axis, with the oxygen moments tilted in the opposite direction to those of the copper, was found to provide the best overall improvement to our refinements.

A diagram of our proposed model is provided in figure 6. Adjacent Cu and O moments are coupled ferromagnetically in the a -direction with a small antiferromagnetically coupled c -axis component. The magnitude and direction of the moments was varied until the lowest

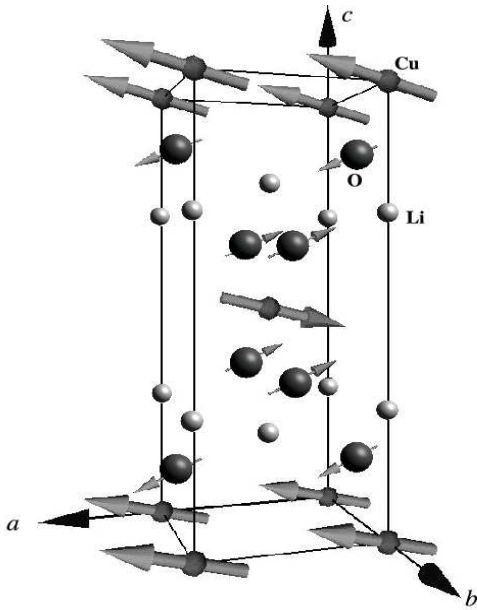


FIG. 6: The antiferromagnetically canted structure found to be most consistent with the observed data.

value of χ^2 was obtained. ($\chi^2=8.75$ with 111 averaged reflections and $\chi^2=6.65$ with the full set of 232 reflections.) The resulting model consisted of $0.91 \mu_B$ Cu moments canted in the a - c plane at an angle of $\theta=76^\circ$ to the c -axis. Oxygen moments approximately $0.12 \mu_B$ in size are counter-canted in the a - c plane at an angle of $\theta=116^\circ$. Although this result suggests that the magnetic structure of Li_2CuO_2 is canted, it should be remembered that a small reduction in χ^2 might also be expected as a side-effect of increasing the number of fitting parameters.

The ordered a -axis moment per formula unit was $1.06 \mu_B$. This is consistent with the $0.96(4) \mu_B$ estimated from powder neutron diffraction¹⁵, and the spin-only value of the free Cu ion ($1 \mu_B$). (For most d -electron transition metal oxides the orbital momentum is expected to be quenched.)

There are also several published estimates for the effective moment per Cu atom obtained from susceptibility measurements. Large discrepancies between these estimates, which vary between $1 \mu_B$ and $2.3 \mu_B$ ^{13,17,29}, are probably due to the combined effects of a preferred [101] orientation of polycrystalline grains, and inappropriate fitting of the data to a Curie-Weiss law. High quality single crystal Li_2CuO_2 susceptibility measurements clearly show that the Curie-Weiss regime ($T \gg J$) does not commence until temperatures well in excess of 300 K^3 .

V. MAGNETISATION DATA

In order to investigate further the nature of the possible canting in Li_2CuO_2 , single-crystal magnetization

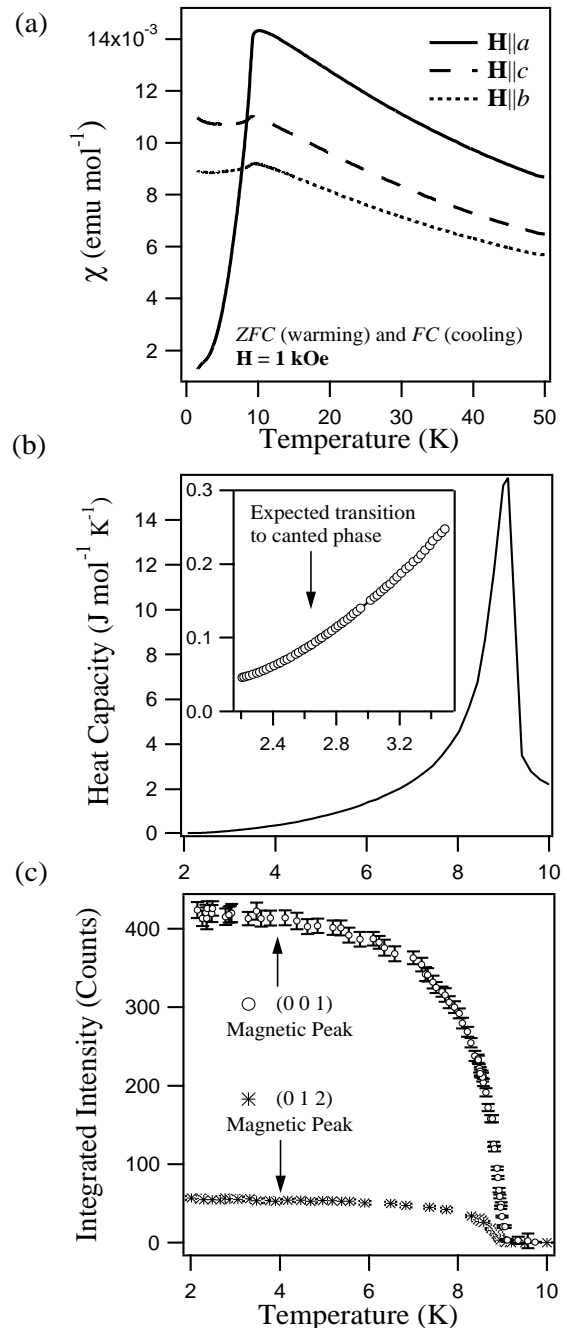


FIG. 7: (a) Li_2CuO_2 single-crystal susceptibility curves measured in $\mathbf{H}=1 \text{ kOe}$ with \mathbf{H} applied parallel to the a , b and c -axes. The crystal was warmed to room temperature and then zero-field-cooled (ZFC) between measurements. Each curve contains data obtained during warming (ZFC data) then cooling of the sample in field (FC data). In 1 kOe no low temperature magnetic transition is observed. (b) Li_2CuO_2 zero-field heat capacity data. Data in the temperature range of the possible transition to the canted phase are shown in the inset. No anomaly in the heat capacity in the region of the transition is observed. (c) Integrated intensities of the (001) and (012) magnetic Bragg peaks measured on warming.

measurements were obtained between 1.6 and 50 K using an Oxford Instruments vibrating sample magnetometer (VSM). The moderately moisture sensitive Li_2CuO_2 crystals were polished to remove surface contamination and then oriented using X-ray Laue photography. By this method the orientation of the crystal axes relative to the applied field could be controlled to within $\pm 5^\circ$. The magnetic properties of three separate crystal specimens weighing 38 mg, 154 mg, and 86 mg were investigated. The latter crystal was deliberately exposed to moisture in order to identify any magnetic impurities arising from surface decomposition; none were observed.

Susceptibility curves obtained along the a , b and c -axes respectively, in an applied field of $\mathbf{H}=1$ kOe, are presented in figure 7(a). These results are in excellent agreement with previous reports^{3,29}. A sharp drop in the susceptibility associated with easy a -axis antiferromagnetic ordering is observed at $T_N = 9 \pm 0.1$ K. Zero-field heat capacity data is presented in figure 7(b). Special care was taken to follow the heat capacity in the vicinity of the expected low temperature transition, 7(b) (inset). The integrated intensities of the (012) and (001) magnetic Bragg peaks are shown in figure 7(c). None of the measurements presented in figure 7 show any visible anomalies in the low-temperature region between 2 and 4 K.

VSM data obtained between $1.6 < T < 20$ K in a weak field of $\mathbf{H} \simeq 20$ Oe are presented in figure 8(a). We find that the response of the bulk crystal to a small applied magnetic field changes abruptly at approximately 2.6 K, producing a small ferromagnetic component in the direction of the field. Below 2.6 K a small ferromagnetic hysteresis was also observed along each of the measured directions, between $-100 < \mathbf{H} < 100$ Oe, figure 8(b).

Although it is possible that the rise in magnetisation could be due to the ordering of a ferromagnetic impurity, the low temperature transition was consistently observed in all three of our samples, and has been reported previously in powder susceptibility¹⁷ and μSR data¹⁶. Assuming that the observed transition is an intrinsic property of the crystal, we find that at ~ 2.6 K the Cu moments, the O moments, (or both), become free to cant toward the applied magnetic field. The observation of ferromagnetic hysteresis when \mathbf{H} is parallel to the a -axis (figure 8(b)), indicates that the moments may not be perfectly aligned along a , even above 2.6 K or in zero field.

VI. DISCUSSION

To conclude, we have performed detailed measurements of the magnetic form-factor of a single crystal of Li_2CuO_2 at 2 K. Patterson analysis of a complete set of unique reflections derived from the observed magnetic diffraction pattern reveals the presence of an effective oxygen moment, which appears to be large and well-localised. Least squares refinement of the magnetic structure in conjunction with the spin-density Patterson analysis reveals that the magnetization densities surrounding

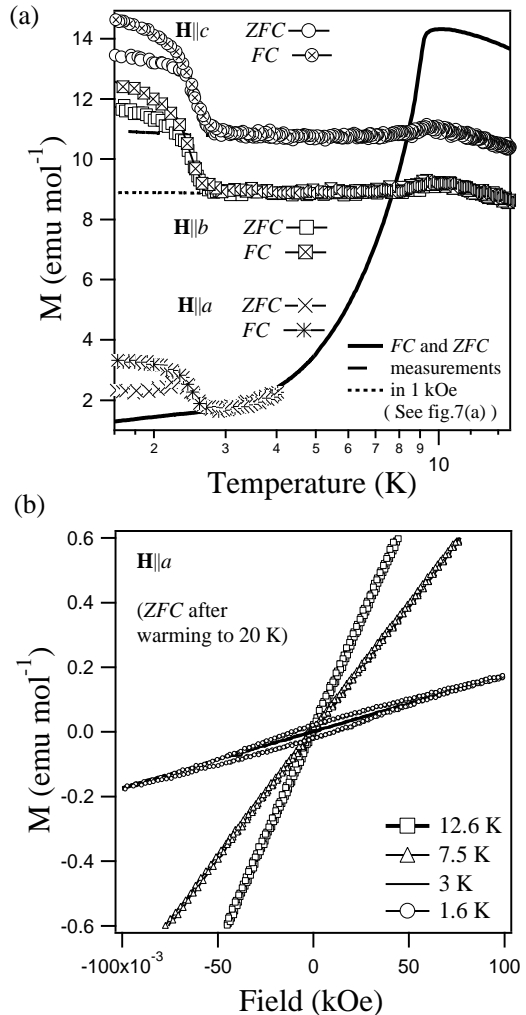


FIG. 8: (a) Li_2CuO_2 susceptibility curves measured in $\mathbf{H}=20$ Oe along the a , b and c -axes. Between each measurement the sample was warmed to at least 20 K and then zero-field cooled (ZFC). Data was then collected during warming in a field of 20 Oe (ZFC), and then on cooling in a field of 20 Oe (FC). The low-field data has been scaled to coincide with the data measured in $\mathbf{H}=1$ kOe (shown as lines), see fig. 7(a). (b) \mathbf{M} - \mathbf{H} loops obtained at 1.6 K, 3 K, 7.5 K and 12.6 K with \mathbf{H} applied parallel to the a -axis.

the Cu and O sites are strongly aspherical. The magnitudes of the O and Cu moments remained approximately stable throughout our refinements. This allows us to estimate that the magnitude of the O moment lies between $0.10 \mu_B$ and $0.12 \mu_B$. These O moments are coupled to Cu moments that are approximately $0.92 \mu_B - 0.96 \mu_B$ in size. Despite the magnitude of the oxygen moment being substantially lower than that estimated by LSDA calculations¹, our observations are otherwise in good qualitative agreement with LSDA predictions for the exchange potential of the FM chain. The size of

the oxygen moment computed using the quantum chemical ‘difference dedicated configuration interaction’ technique for Li_2CuO_2 is closer to that measured in this experiment⁵.

Although large covalency effects have been observed previously in structures such as K_2IrCl_6 ⁹, reports of moment formation in oxides are extremely rare. The oxygen moment in Li_2CuO_2 is one of the largest so far recorded, rivaled in size only by the $0.1 \mu_B$ moment suggested to reside on the oxygen sites in the ferromagnetic manganite $\text{La}_{0.8}\text{Sr}_{0.2}\text{MnO}_3$ ³⁰. (In the polarized neutron study of the manganite an oxygen moment was identified, but attempts to refine its magnitude from the measured structure factors proved unsuccessful.) In other examples of oxygen moment formation the transfer of moment from the magnetic ion to the oxygen site has been shown to be much smaller. For example, the only confirmed oxygen moment in a cuprate system is of $0.02 \mu_B$ in the chain-ladder compound $\text{La}_{14-x}\text{Ca}_x\text{Cu}_{24}\text{O}_{41}$ ³¹.

Besides the discovery of the O moment in Li_2CuO_2 , our observations also seem consistent with the notion of canting. A ferromagnetic-like rise in the magnetization of our single-crystal samples was verified by low-field ($\mathbf{H} = 20$ Oe) magnetization measurements to occur at $T = 2.6 \pm 0.2$ K. However, since many possible configurations of canted Cu and O moments may be compatible within error with the observed magnetic diffraction pattern, it is difficult to reach any reliable conclusions about the nature of the canting. Having restricted our refinements to antiferromagnetic canted configurations, our most successful model of the observed data consists of ~ 0.91

μ_B Cu moments canted in the a - c plane at an angle of $\theta=76^\circ$ to the c -axis. Nearest neighboring $0.12 \mu_B$ O moments are ferromagnetically coupled to the Cu along a , but counter-canted at an angle of $\theta=116^\circ$ from c , (see also figure 6).

Previous researchers¹ have suggested that the Cu d_{yz} and O p_σ orbitals, which extend along the magnetic ribbons, are energetically isolated and strongly hybridized. Covalency effects serve to polarize the neighboring oxygen ions, resulting in a large net transfer of the Cu moment to the oxygen sites. In Li_2CuO_2 we find that the Cu moment is large and well separated from that of the O. Counter-canting of adjacent oxygen moments seems inconsistent with the idea of a purely polarization-induced oxygen magnetization, and it is possible that the true magnetic structure of Li_2CuO_2 may be frustrated, ferromagnetically canted or more complicated than our proposed model. (A ferromagnetically canted configuration of moments would have contributed a slight intensity to the nuclear peaks and was therefore difficult to refine using our existing data.) In order to determine the nature of configuration of any canted phase with more confidence further experiments are required.

VII. ACKNOWLEDGEMENTS

The authors thank Julie Staunton, Martin Boehm, Jim Hague, Clive Wilkinson and Jane Brown for useful discussions, and the Engineering and Physical Sciences Research Council, UK, for financial support.

-
- ¹ R.Weht and W.E.Pickett, Phys. Rev. Lett. **81**, 2502 (1998).
 - ² R.Neudert, H.Rosner, S-L.Drehsler, M.Kielwein, M.Sing, Z.Hu, M.Knupfer, M.S.Golden, J.Fink, N.Nucker, et al., Phys.Rev.B **60**, 13413 (1999).
 - ³ Y.Mizuno, T.Tohyama, S.Maekawa, T.Osafune, N.Motoyama, H.Eisaki, and S.Uchida, Phys. Rev. B **57**, 5326 (1998).
 - ⁴ B.Delley, H.B.Braun, B.Roessli, A.Amato, and U.Staub, PSI Scientific report **III**, 78 (1999).
 - ⁵ C. de Graaf, I. de P.R. Moreira, F. Illas, Ó.Iglesias, and A. Labarta, Phys. Rev. B **66**, 014448 (2002).
 - ⁶ J.B.Goodenough, Phys. Rev. **100**, 564 (1955).
 - ⁷ J.Kanamori, J. Phys. Chem. Solids **10**, 87 (1959).
 - ⁸ P.W.Anderson, Solid State Phys. **14**, 99 (1963).
 - ⁹ J.W.Lynn, G.Shirane, and M.Blume, Phys. Rev. Lett. **37**, 154 (1976).
 - ¹⁰ R.Hoppe and H.Riek, Z. Anorg. Allg. Chem. **379**, 157 (1970).
 - ¹¹ H. Ohta, N. Yamauchi, T. Nanba, M. Motokawa, S. Kawamura, and K. Okuda, J. Phys. Soc. Jpn. **62**, 785 (1993).
 - ¹² K.Shreedhar and P.Ganguly, Inorg. Chem. **27**, 2261 (1988).
 - ¹³ K.Okuda, S.Noguchi, K.Konishi, H.Degchi, and K.Takeda, J. Magn. Magn. Mater. **104**, 817 (1992).
 - ¹⁴ R.Hoffmann, R.Hoppe, and W.Schäfer, Z. Anorg. Allg. Chem. **578**, 18 (1989).
 - ¹⁵ F.Sapiña, J.Rodriguez-Carvajal, M.J.Sanchis, R.Ibanez, A.Beltran, and D.Beltran, Solid State Commun. **74**, 779 (1990).
 - ¹⁶ U.Staub, B.Roessli, and A.Amato, Physica B **289-290**, 299 (2000).
 - ¹⁷ R.J.Ortega, P.J.Jensen, K.V.Rao, F.Sapiña, D.Beltran, Z.Iqbal, J.C.Cooley, and J.L.Smith, J. Appl. Phys. **83**, 6542 (1998).
 - ¹⁸ S.Patat, D.P.Blunt, A.M.Chippendale, and P.G.Dickens, Solid State Ionics **46**, 325 (1991).
 - ¹⁹ C.Wilkinson, H.W.Khamis, R.F.D.Stansfield, and G.J.McIntyre, J. Appl. Crystallography. **21**, 471 (1988).
 - ²⁰ P.Coppens, L.Leiserowitz, and D.Rabinovich, Acta Crystallogr. **18**, 1035 (1965).
 - ²¹ P.J.Becker and P.Coppens, Acta Crystallogr. **A30**, 129 (1974).
 - ²² P.J.Brown, *International Tables for Crystallography* (Kluwer Academic Publishers, Dordrecht, 1992), vol. C, chap. 4.4.5, p. 230.
 - ²³ C.Wilkinson, Phil. Mag. **17**, 609 (1968).
 - ²⁴ C.Wilkinson, Acta Crystallogr. **A29**, 449 (1973).
 - ²⁵ C.Wilkinson and E.J.Lisher, Acta Crystallogr. **A29**, 453 (1973).
 - ²⁶ O.Halpern and M.H.Johnson, Phys. Rev. **55**, 898 (1939).

- ²⁷ P.J.Brown and J.C.Matthewman, Tech. Rep., Rutherford Appleton Laboratory (1993).
- ²⁸ P.J.Brown (2000), private communication.
- ²⁹ M.Boehm, S.Coad, B.Roessli, A.Zheludev, M.Zolliker, P.Boni, D.McK.Paul, H.Eisaki, N.Motoyama, and S.Uchida, Europhys. lett. **43**, 77 (1998).
- ³⁰ J.Pierre, B.Gillon, L.Pinsard, and A.Revcolevschi, Europhys. Lett. **42**, 85 (1998).
- ³¹ M.Matsuda, K.M.Kojima, Y.L.Uemura, J.L.Zaretsky, K.Nakajima, K.Kakurai, T.Yokoo, S.M.Shapira, and G.Shirane, Phys. Rev. B **57**, 11467 (1998).